Supporting Information

Assembly of four new cobalt coordination polymers modulated by N-coligands: sensitive and selective sensing of nitroaromatics, Fe^{3+} and $Cr_2O_7^{2-}$ in water

Qian-Qian Tu[a], Ling-Ling Ren[a], Ying-Ying Cui[a], Ai-Ling Cheng[*a] , En-Qing Gao[b]

[a] *College of Chemistry and Molecular Engineering, East China Normal University, Shanghai 200240, People's Republic of China.*

[b] *Shanghai Key Laboratory of Green Chemistry and Chemical Processes, College of Chemistry and Molecular Engineering, East China Normal University, Shanghai 200062, People's Republic of China.*

Table of Contents

S1. General methods

FT-IR spectra were recorded on a Nicolet NEXUS 670 spectrophotometer using KBr pellets in the range of 500–4000 cm^{-1}. Thermogravimetric analyses (TGA) were carried out on a Mettler

Toledo TGA/SDTA851 instrument with a heating rate of 5 °C/min under nitrogen atmosphere. Powder X-ray diffraction (PXRD) patterns were collected on a Rigaku ULTIMA IV diffractometer equipped with Cu Kα in a 2θ range of 5–40°. Elemental analyses (C, H and N) were performed on an Elementar Vario ELIII analyzer. Fluorescence spectra were recorded at room temperature with an Edinburgh FLS980 fluorescence spectrophotometer. UV-visible absorption spectra were measured on a Cary 100 Bio UV-visible Spectrophotometer.

S2. X-ray Crystallography.

Diffraction intensity data for **1** to **4** were collected on a Bruker Apex II CCD area detector equipped with graphite-monochromated Mo-Kα radiation (λ = 0.71073 Å) at 293K. Empirical absorption correction was applied using the SADABS program. The structures were solved by direct methods and refined by the full-matrix least-squares based on F^2 using SHELXTL. The non-hydrogen atoms were refined anisotropically, and the hydrogen atoms of the ligands were placed in calculated positions and refined using a riding model. Notably, methoxy groups on the L^{2-} ligands are disordered over two positions. Besides, L^{2-} ligands in the single linkers in **2** and **3** are also disordered over two positions. The solvent molecules in **2**–**4** are highly disordered and could not be modeled correctly, so the residual electron densities resulting from them were removed by the SQUEEZE function in PLATON, and the resultant new files were used to further refine the structures.

S3. Explanation for the Alert B in the CheckCIF reports

1. ALERT_B in CheckCIF report of CP 2~4

Alert level B

PLAT990_ALERT_1_B Deprecated .res/.hkl Input Style SQUEEZE Job ... ! Note

Explanation: This alert comes from the use of squeeze programme of Platon sofeware.

2. Alert-B in CheckCIF report of CP 2

Alert level B

RINTA01_ALERT_3_B The value of Rint is greater than 0.18

Rint given 0.205

PLAT020_ALERT_3_B The Value of Rint is Greater Than 0.12 ..... 0.205 Report

PLAT084_ALERT_3_B High wR2 Value (i.e. > 0.25) ..... 0.42 Report

Explanation: These alerts come from the poor quality of the crystal data and the large amounts of disorder in the structure. We have tried our best to re-collect the data but without success. This structure was included for comparison with the complex 3. We are confident that the structural characterization is valid.

PLAT213_ALERT_2_B Atom C24 has ADP max/min Ratio ..... 4.5 prolat

PLAT214_ALERT_2_B Atom C34 (Anion/Solvent) ADP max/min Ratio 5.2 prolat

PLAT220_ALERT_2_B Non Solvent Resd 1 C Ueq(max) / Ueq(min) Range 8.0 Ratio

PLAT341_ALERT_3_B Low Bond Precision on C-C Bonds ..... 0.01544 Ang.

Explanation: These alerts come from the large amount of disorder in the structure.

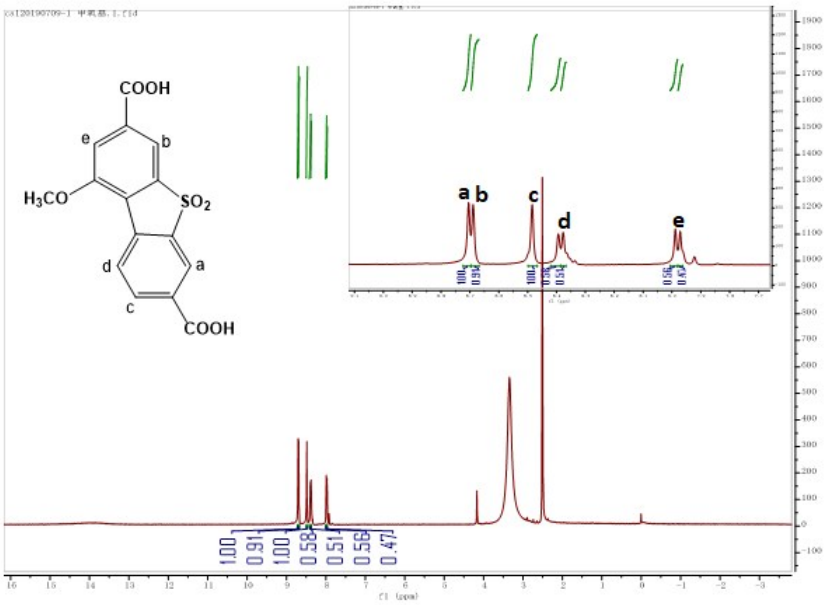

Figure S1. ^{1}H-NMR (DMSO) spectrum of H_2L.

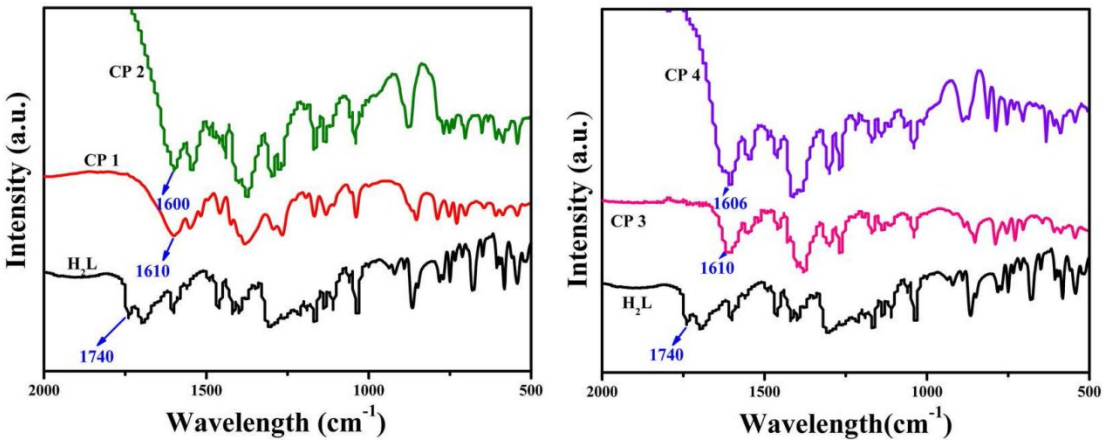

Figure S2. IR spectra of H_2L ligand, complexes **1** to **4**.

Table S1. Crystal data and structural refinements for **1**–**4**.

Complexes	**1**	**2**	**3**	**4**
Formula	$CoC_{27}H_{18}O_8N_2S$	$Co_3C_{69}H_{48}O_{25}N_4S_3$	$Co_3C_{65}H_{56}O_{29}N_4S_3$	$Co_2C_{60}H_{60.5}O_{19.5}N_{6.5}S_2$
Fw	589	1606	1630	1367
T (K)	293(2)	293(2)	293(2)	293(2)
Crystal system	Triclinic	Triclinic	Triclinic	Orthorhombic
space group	$P\bar{1}$	$P\bar{1}$	$P\bar{1}$	*Pbam*
a (Å)	7.4557(3)	10.8048(4)	10.5883(4)	17.876(2)
b (Å)	12.6096(5)	12.8422(7)	12.9921(5)	27.491(2)
c (Å)	13.7586(3)	14.3174(5)	14.4442(5)	11.3809(10)
α (°)	94.478(3)	65.558(4)	63.887(4)	90
β (°)	98.662(3)	81.826(3)	79.260(3)	90
γ (°)	101.166(3)	79.139(4)	79.327(3)	90
V (Å)	1246.84(8)	1771.62(14)	1740.90(13)	5593.0(9)
Z	5	8	7	24
D_{calcd} (g·cm^{-3})	1.57	1.438	1.417	0.65
F (000)	602	779	55	1116
GOF on F^2	1.036	1.247	1.085	0.93
R (int)	0.0505	0.2048	0.0665	0.1614
R_1 [$I > 2\sigma(I)$]	0.0456	0.1469	0.0881	0.0848
wR_2 (all data)	0.1217	0.4196	0.2134	0.2721

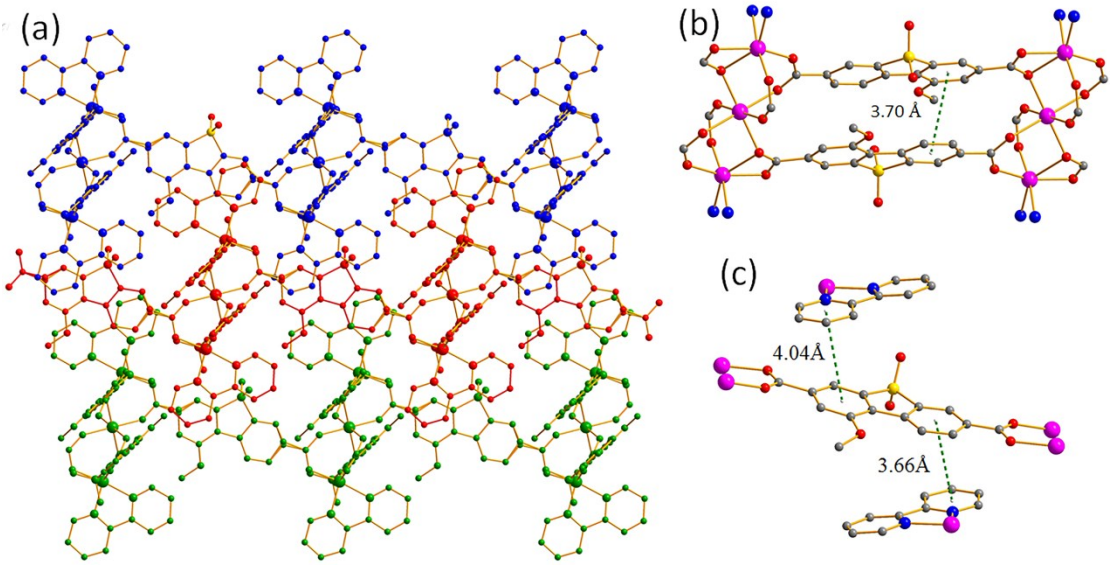

Figure S3. Molecular structure of **3**. (a) packing of the layers; (b) π–π stacking between phenyl rings of $L^{2-}\cdots L^{2-}$ pairs within the layer; (c) π–π stacking between pyridyl ring of 2,2'-bipy and phenyl of L^{2-} from adjacent layers.

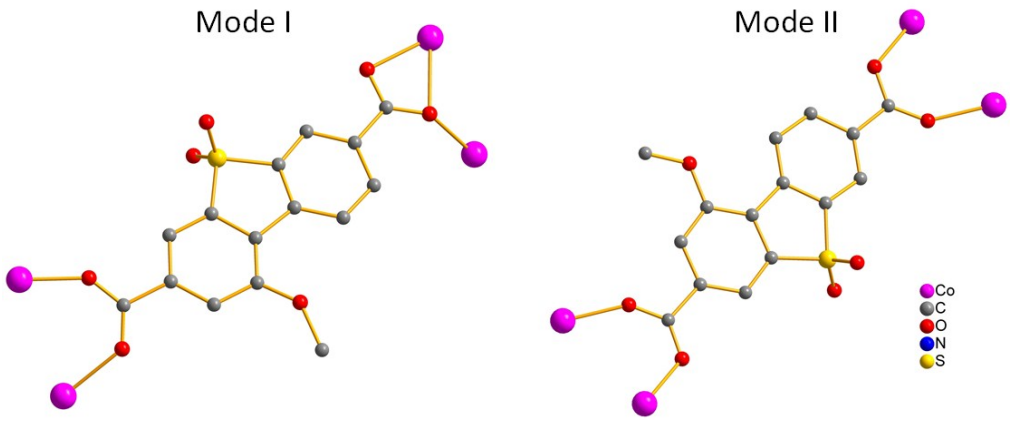

Figure S4. The coordination modes of L^{2-} ligand in complex **2** and **3**.

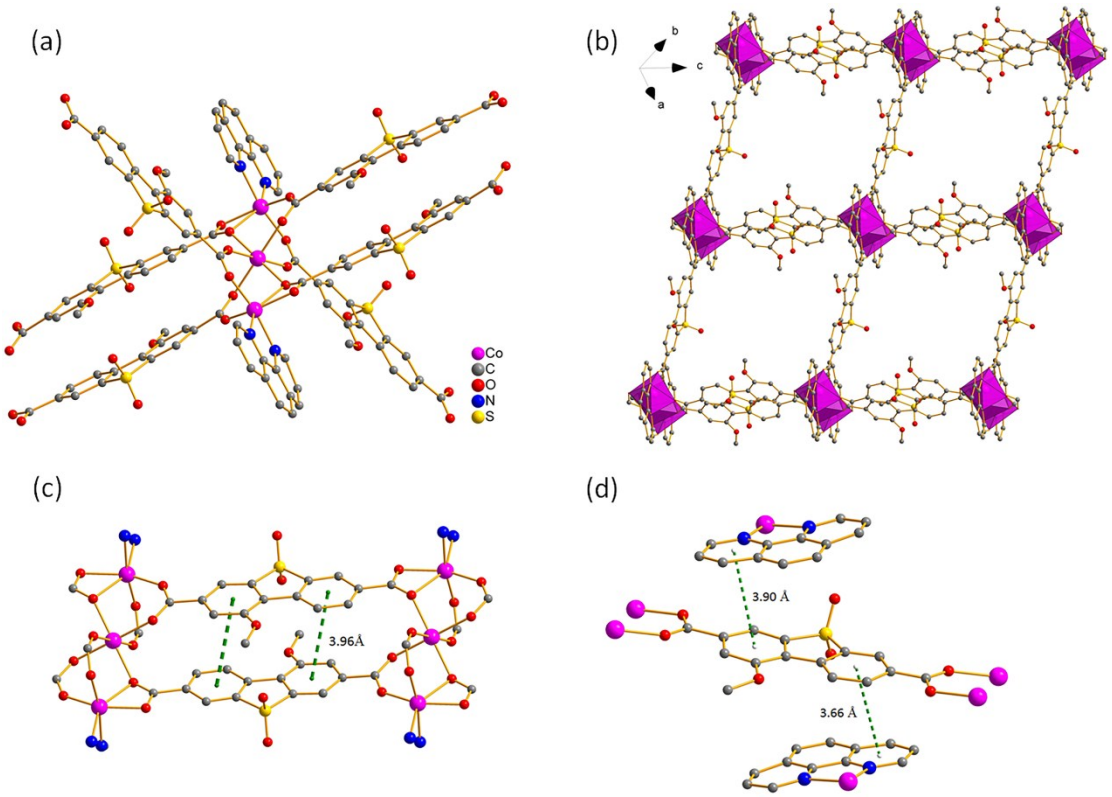

Figure S5. Molecular structure of complex **2**. (a) building unit showing the coordination environment of Co centers; (b) Infinite 2D (4,4) network; (c) π–π stacking between phenyl rings of L^{2-}···L^{2-} pairs within the layer; (d) π-π stacking between pyridyl ring of phen and phenyl of L^{2-} from adjacent layers.

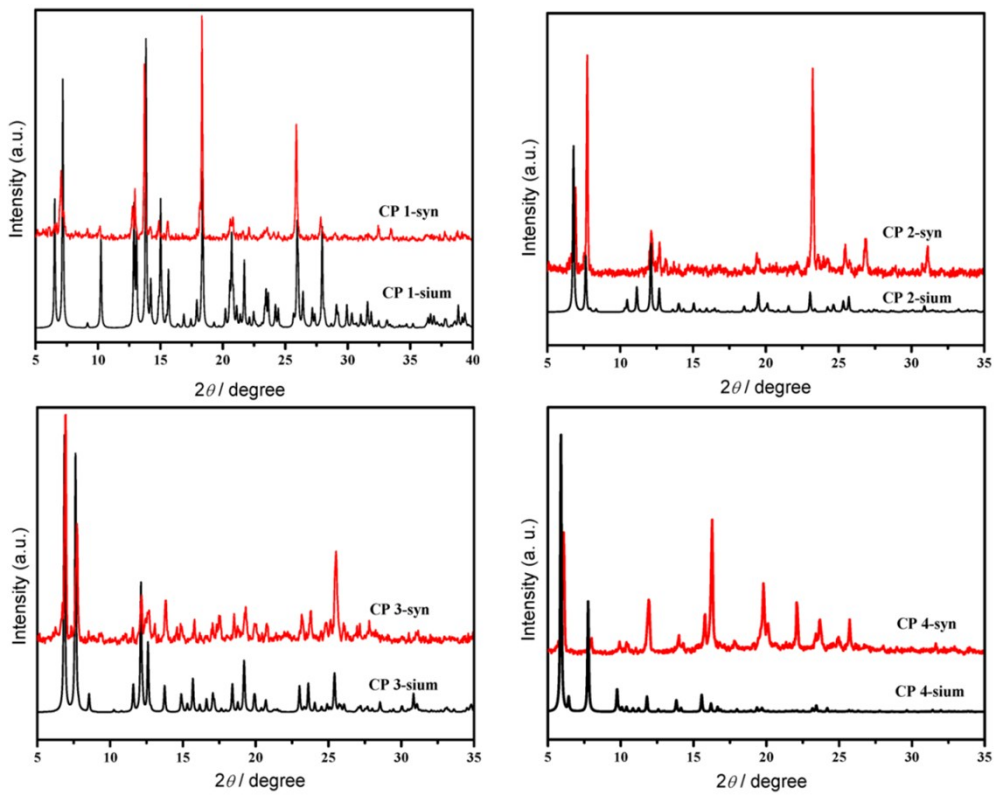

Figure S6. PXRD patterns of **1** to **4** (simulated from single-crystal X-ray data and experimental data).

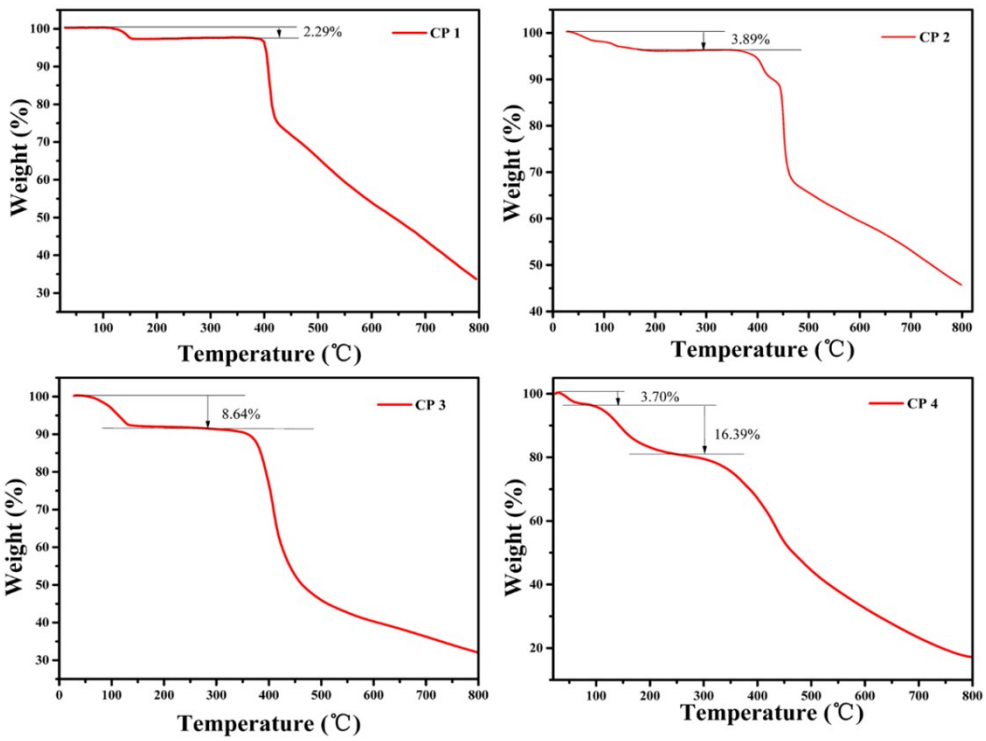

Figure S7. TGA curves of complexes **1** to **4**.

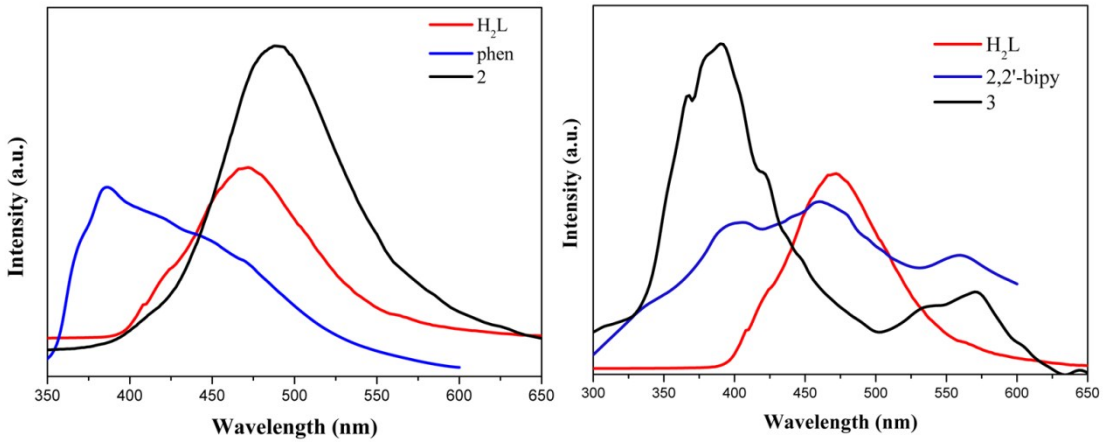

Figure S8. Solid-state emission spectra of complexes **2** (a) and **3** (b) at 293k (λ_{ex} = 292nm).

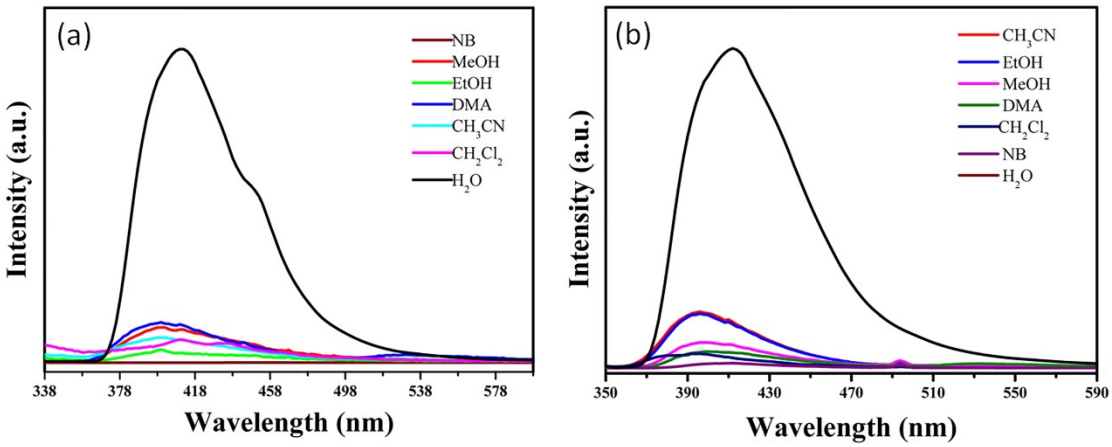

Figure S9. Emission spectra of complexes **2** (a) and **3** (b) dispersed in different solvents (λ_{ex} = 340 nm).

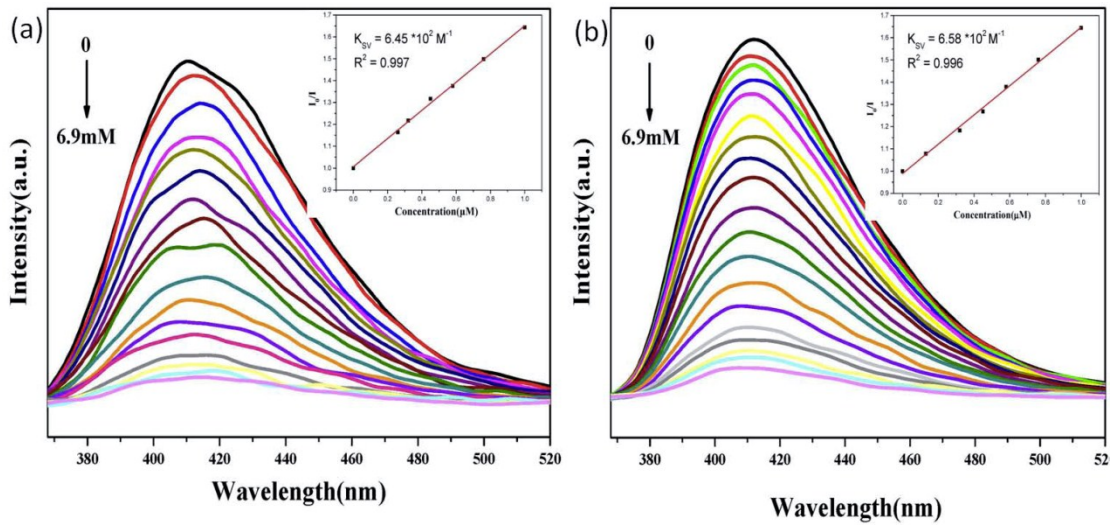

Figure S10. Emission spectra of **2** (a) and **3** (b) upon incremental addition of PNT. Inset: Linear plot of I_0/I at low concentration of PNT.

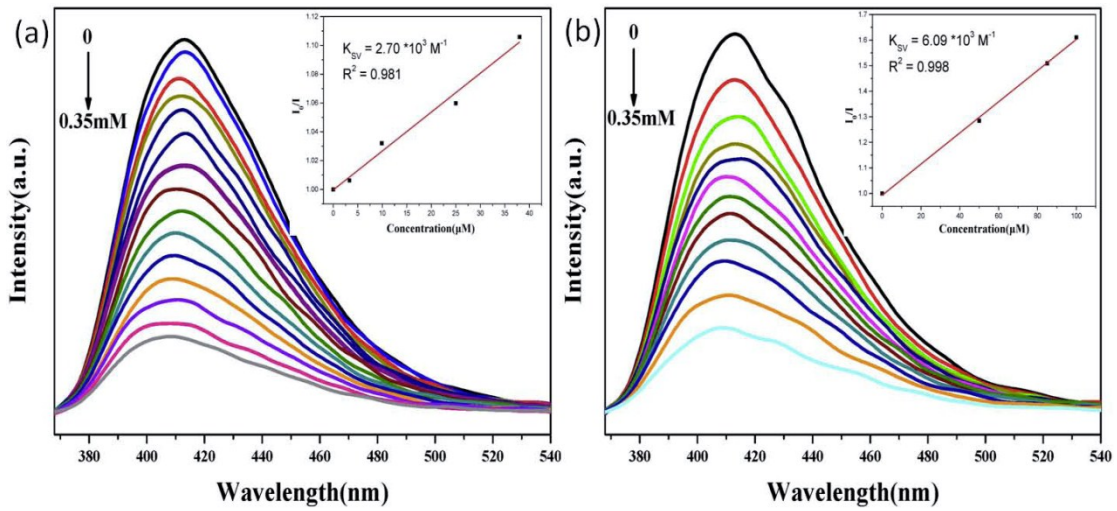

Figure S11. Emission spectra of **2** (a) and **3** (b) upon incremental addition of PNP. Inset: Linear plot of I_0/I at low concentration of PNP.

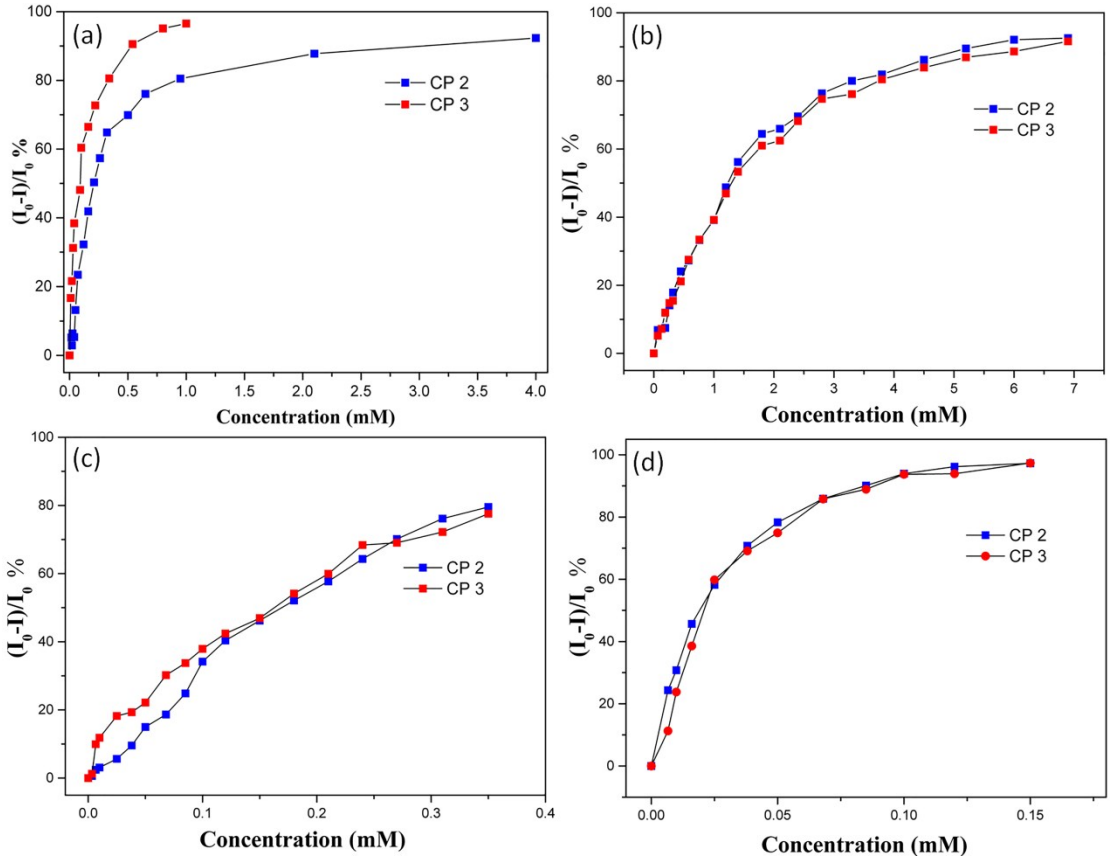

Figure S12. The corresponding quenching efficiency of CPs **2** and **3** towards NB (a), PNT (b), PNP (c), and DNP (d) in H_2O.

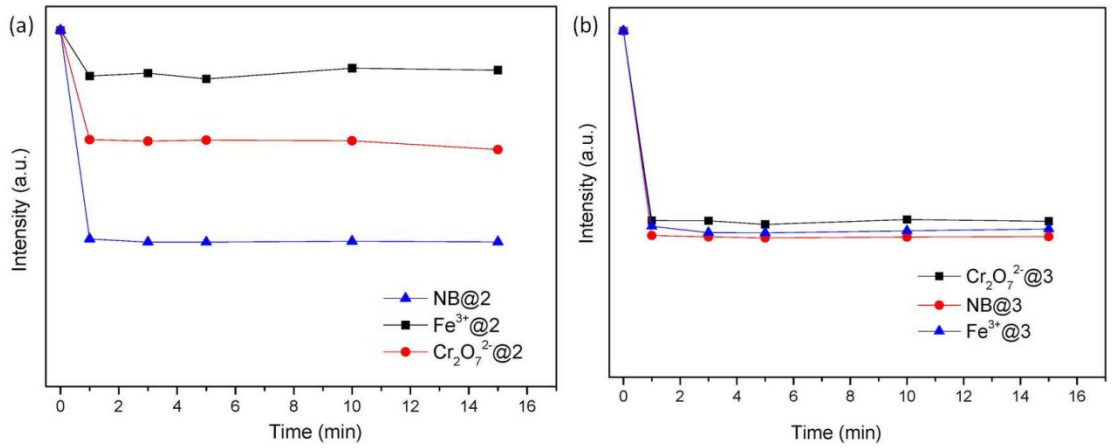

Figure S13. Response time of **2** (a) and **3** (b) towards NB, Fe^{3+} and $Cr_2O_7^{2-}$.

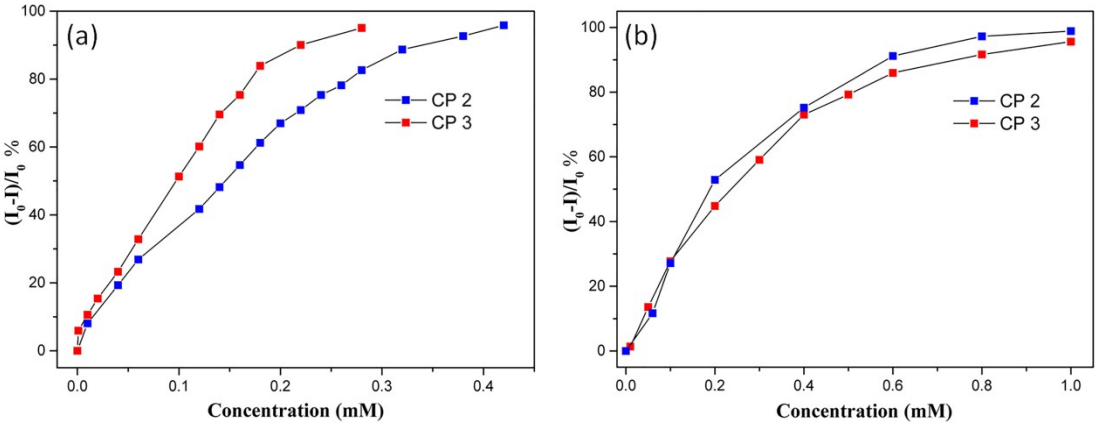

Figure S14. The corresponding quenching efficiency of CPs **2** and **3** towards Fe^{3+} (a) and $Cr_2O_7^{2-}$ (b) in H_2O.

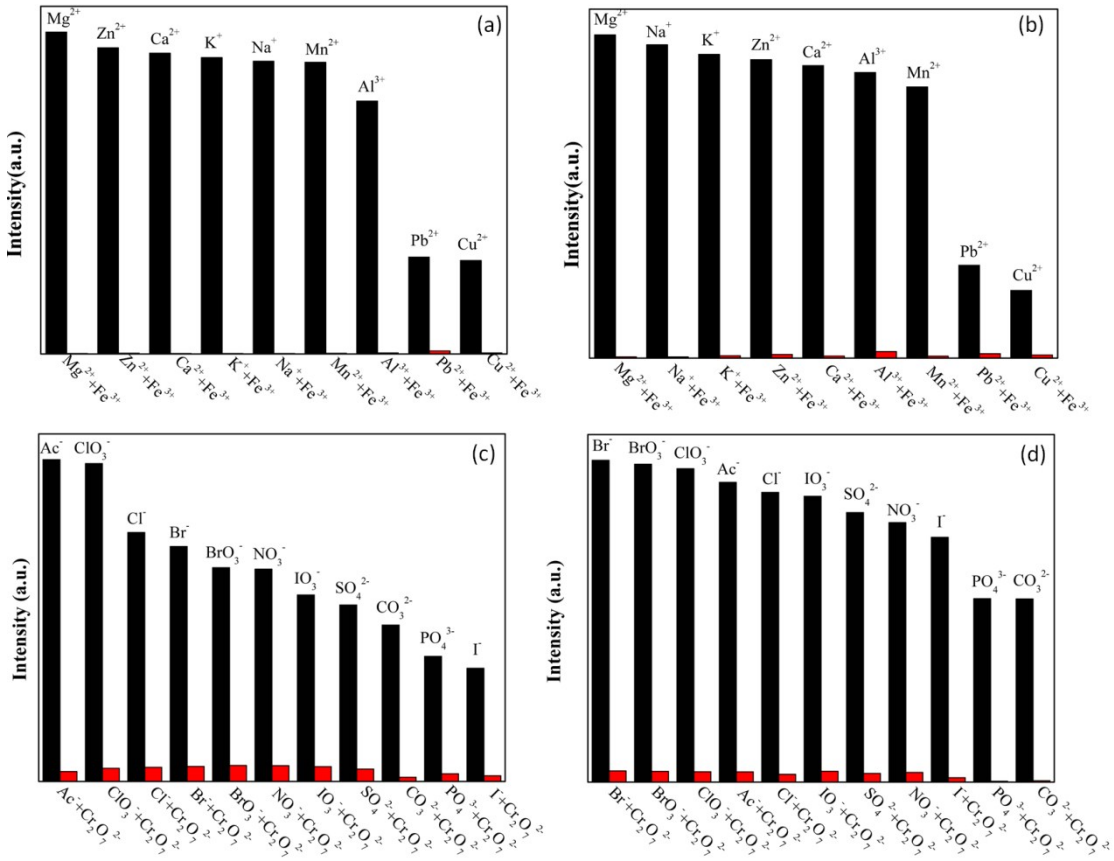

Figure S15. Comparison of the photoluminescence intensities of **2** (a) and **3** (b) in H_2O suspensions with the introduction of other interfering metal ions and anions.

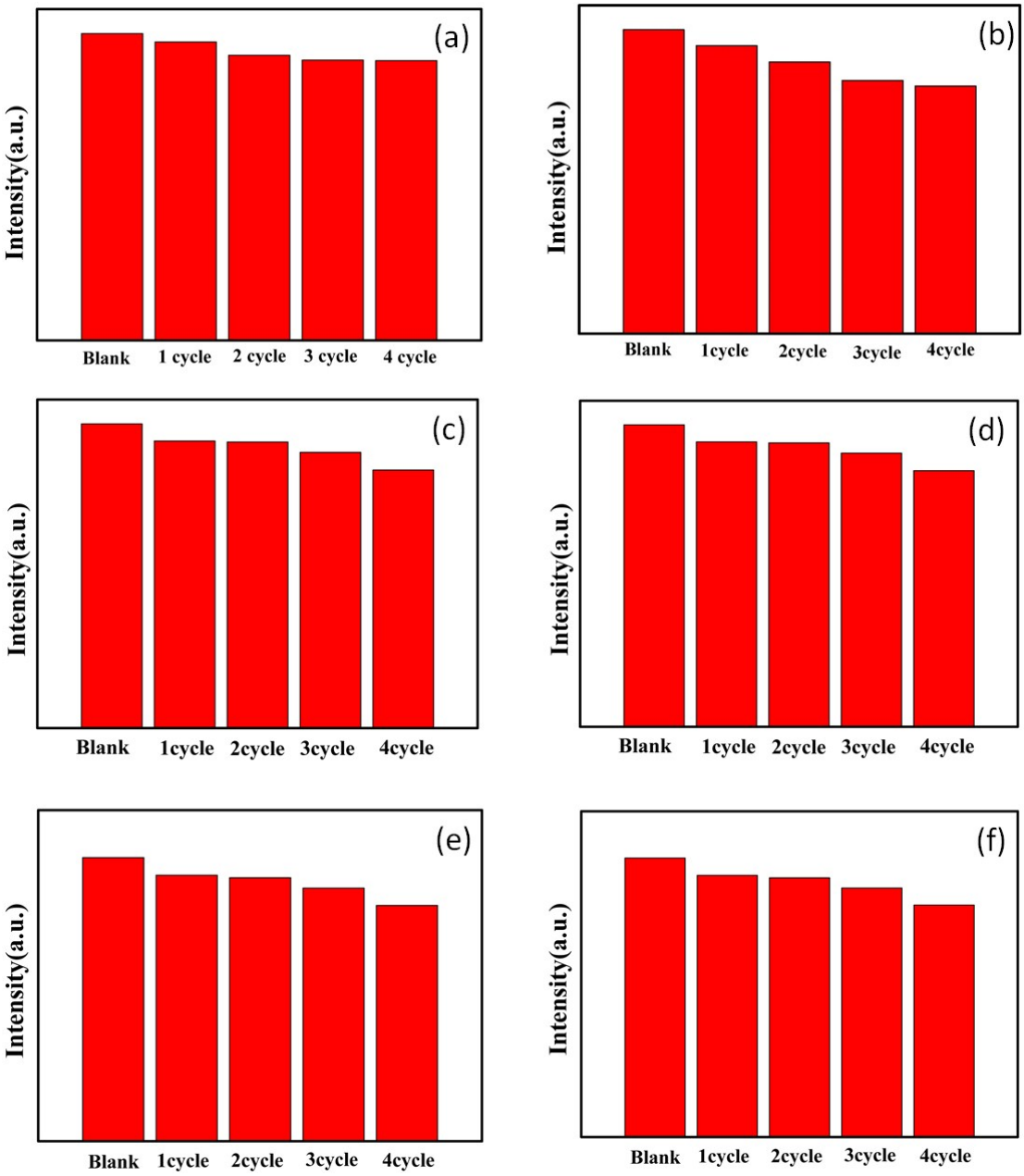

Figure S16. Fluorescence intensities of **2** and **3** in four recyclable experiments for sensing NB (a, b), Fe^{3+} (c, d), $Cr_2O_7^{2-}$ (e, f) in H_2O.

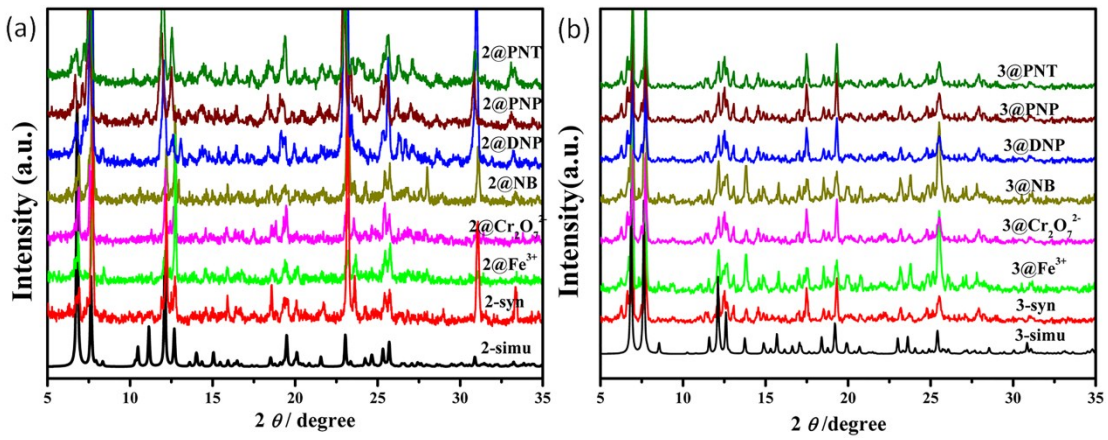

Figure S17. The PXRD patterns of **2** (a) and **3** (b) after detection of NB, Fe^{3+}, and $Cr_2O_7^{2-}$.

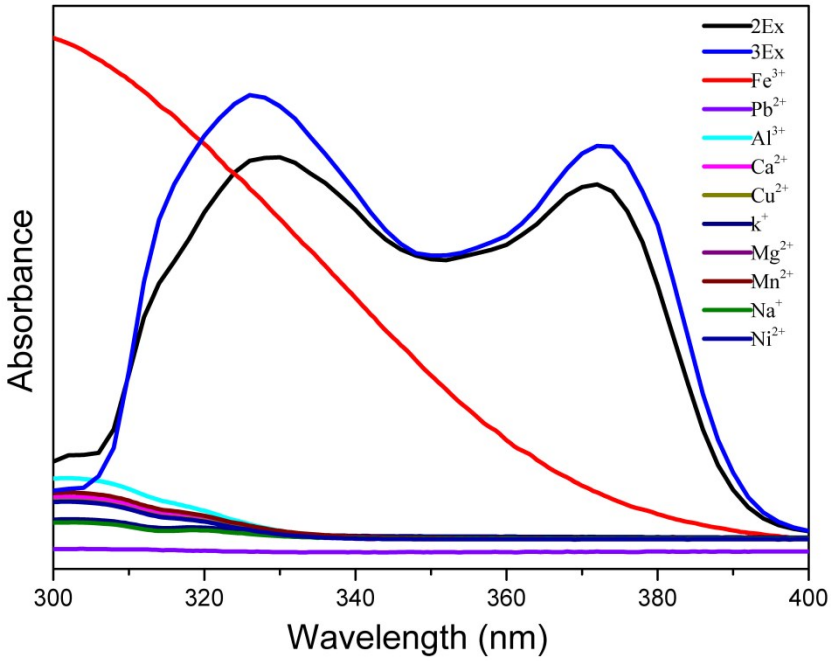

Figure S18. UV-Vis absorption spectra of various metal ion aqueous solutions and the excitation spectra of **2** and **3**.

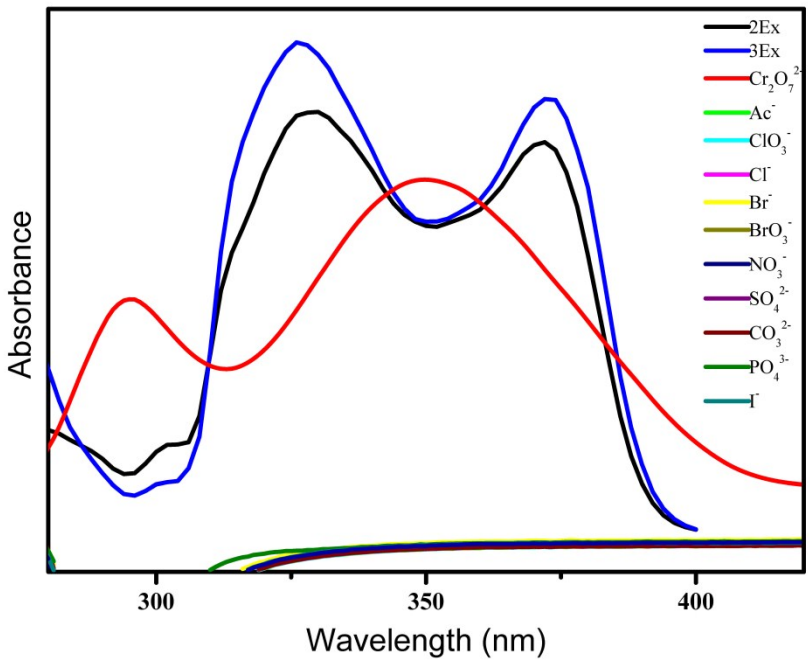

Figure S19. UV-Vis absorption spectra of various anion aqueous solutions and the excitation spectra of **2** and **3**.

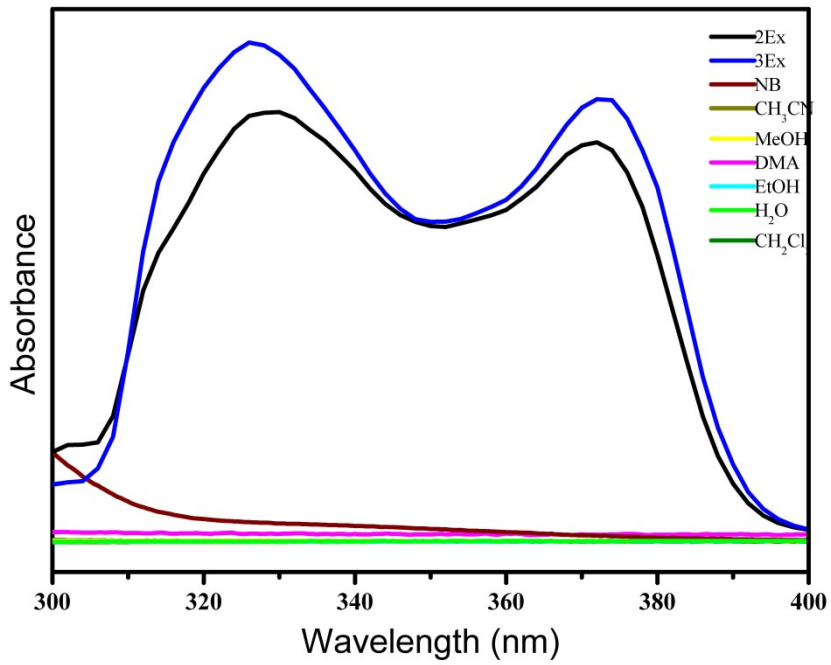

Figure S20. UV-Vis absorption spectra of various solvent molecules and the excitation spectra of **2** and **3**.

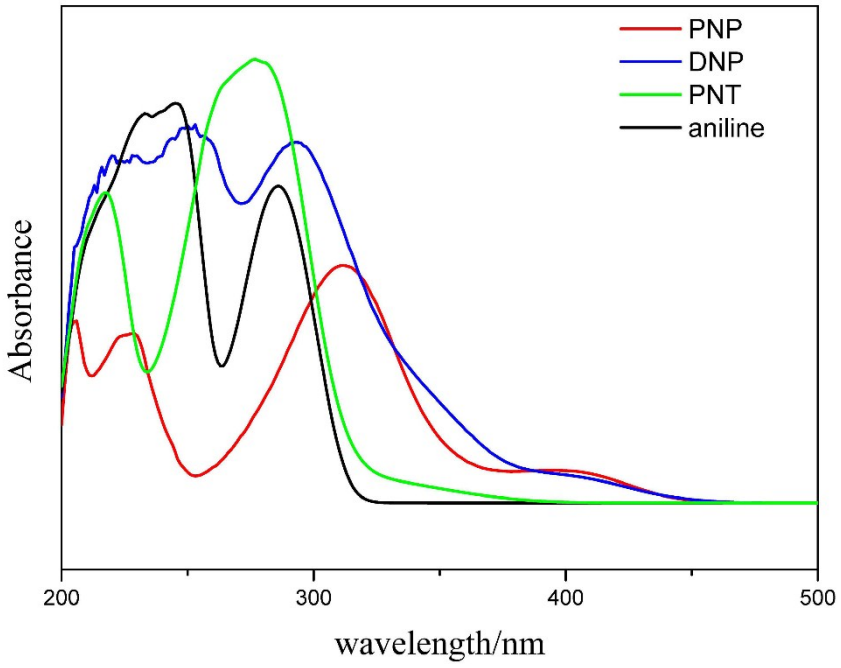

Figure S21. UV-Vis absorption spectra of various NACs EtOH solutions.

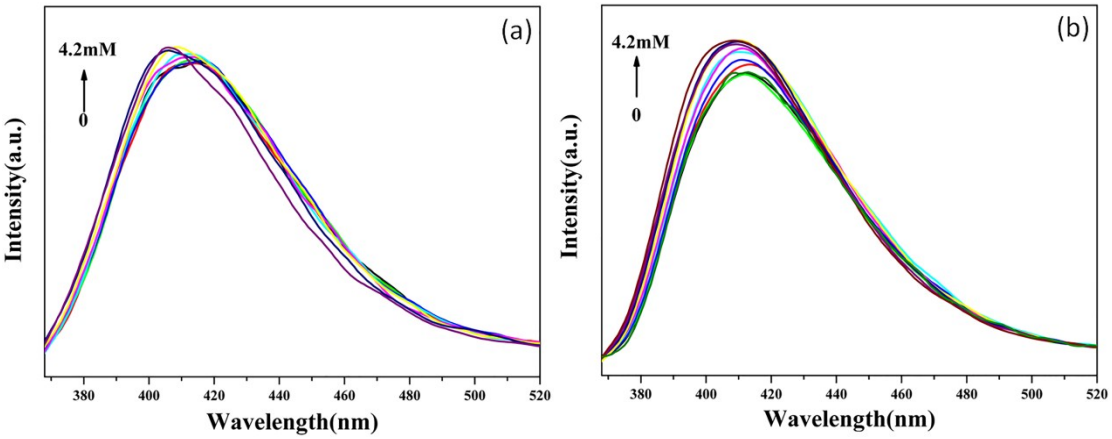

Figure S22. Emission spectra of **2** (a) and **3** (b) upon incremental addition of aniline.

Table S2. Comparison of detection ability of **2** and **3** with other CPs based materials towards NB.

CPs/MOFs materials	Quenching Constant (M^{-1})	Detection limits	Solvent	Recycl ability	Ref.
CP 2	4.22×10^3	18.2 μM	water	yes	This work
CP 3	1.49×10^4	5.4 μM	water	yes	This work
$[Zn(TIPA)pim_{0.5}]2H_2O \cdot NO_3$	6.18×10^3		DMF		1
$[Zn_2(L)(5\text{-}AIP)_2] \cdot 3H_2O$	6.7×10^3		water		2
$[Zn_3(mtrb)_3(btc)_2] \cdot 3H_2O$	2.88×10^3		MeOH		3
$[Tb(HL)(H_2O)_2(NO_3)] \cdot NO_3$	2.6×10^4	18 μM	DMF		4
$[Tb(DMTDC)_{1.5}(H_2O)_2] \cdot DEF$	9.34×10^4	17 μM (2.1 ppm)	DMF		5

Table S3. Comparison of detection ability of **2** and **3** with other CPs based materials towards Fe^{3+}.

CPs/MOFs materials	Quenching Constant (M^{-1})	Detection limits	Solvent	Recycl ability	Ref.
CP 2	8.10×10^3	9.39 μM	water	yes	This work
CP 3	6.27×10^3	11.4 μM	water	yes	This work
$[Zn_2(L)(5\text{-}AIP)_2] \cdot .2CH_3OH$	4.475×10^3	1.29 μM	water	yes	2
$[Zn_3(mtrb)_3(btc)_2] \cdot 3H_2O$	6.50×10^3	1.78 μM.	water	yes	3
$[Eu_3(pdba)_4(H_2O)_4] \cdot 5H_2O$	5.76×10^3		water		6
Tb-DSOA	3.54×10^3		water		7
BUT-14	2.17×10^3	3.8 μM	water		8
$[Tb(Cmdcp)(H_2O)_3] \cdot NO_3 \cdot 2.5H_2O$	5.53×10^3	4.0 μM			9
$Cu_3(CN)_3(MPTZ)$	1.07×10^4	2.0 μM	DMF		10

Table S4. Comparison of detection ability of **2** and **3** with other CPs based materials towards $Cr_2O_7^{2-}$.

CPs/MOFs materials	Quenching Constant (M^{-1})	Detection limits	Solvent	Recycl ability	Ref.
CP 2	5.62×10^3	16.6 μM	water	yes	This work
CP 3	4.13×10^3	21.2 μM	water	yes	This work
$[Cd(L)(SDBA)(H_2O)]\cdot 0.5H_2O$	4.97×10^3	48.6μM	water		11
$[Zn(L1)(H_2O)]\cdot H_2O$	6.32×10^3	4.1μM	water		12
$[Cd(L)(4,4\text{-bpy})]\cdot DMF\cdot H_2O$	2.83×10^3	7.1μM	DMF	yes	13
$[Zn_2(ttz)H_2O]$	2.19×10^3		water	yes	14
$[Zn_2(TPOM)(BDC)_2]\cdot 4H_2O$	4.45×10^3	3.9 μM	DMF	yes	15
$[Eu(Hpzbc)_2(NO_3)]\cdot H_2O$		22 μM	EtOH		16

Reference

1. X.-Q. Yao, G.-B. Xiao, H. Xie, D.-D. Qin, H.-C. Ma, J.-C. Liu and P.-J. Yan, *CrystEngComm*, 2019, **21**, 2559-2570.
2. D. Das and K. Biradha, *Crystal Growth & Design*, 2018, **18**, 3683-3692.
3. Y. Q. Zhang, V. A. Blatov, T. R. Zheng, C. H. Yang, L. L. Qian, K. Li, B. L. Li and B. Wu, *Dalton Trans*, 2018, **47**, 6189-6198.
4. W. Gao, F. Liu, B. Y. Zhang, X. M. Zhang, J. P. Liu, E. Q. Gao and Q. Y. Gao, *Dalton Trans*, 2017, **46**, 13878-13887.
5. S. Wang, T. Cao, H. Yan, Y. Li, J. Lu, R. Ma, D. Li, J. Dou and J. Bai, *Inorganic chemistry*, 2016, **55**, 5139-5151.
6. H. Li, Y. Han, Z. Shao, N. Li, C. Huang and H. Hou, *Dalton Transactions*, 2017, **46**, 12201-12208.
7. X. Y. Dong, R. Wang, J. Z. Wang, S. Q. Zang and T. C. W. Mak, *Journal of Materials Chemistry A*, 2015, **3**, 641-647.
8. B. Wang, Q. Yang, C. Guo, Y. X. Sun, L. H. Xie and J. R. Li, *Acs Applied Materials & Interfaces*, 2017, **9**, 10286-10295.
9. K. Y. Wu, L. Qin, C. Fan, S. L. Cai, T. T. Zhang, W. H. Chen, X. Y. Tang and J. X. Chen, *Dalton Trans*, 2019, **48**, 8911-8919.
10. Y. Gai, X. Zhao, Y. Chen, S. Yang, X. Xia, S. Liu, X. Wan and K. Xiong, *Dalton Trans*, 2018, **47**, 6888-6892.
11. S. G. Chen, Z. Z. Shi, L. Qin, H. L. Jia and H. G. Zheng, *Crystal Growth & Design*, 2017, **17**, 67-72.
12. K. K. Wan, J. H. Yu and J. Q. Xu, *Crystengcomm*, 2019, **21**, 3086-3096.
13. Z. W. Chen, X. N. Mi, J. Lu, S. N. Wang, Y. W. Li, J. M. Dou and D. C. Li,

Dalton Transactions, 2018, **47**, 6240-6249.

14. C. S. Cao, H. C. Hu, H. Xu, W. Z. Qiao and B. Zhao, *Crystengcomm*, 2016, **18**, 4445-4451.
15. R. Lv, J. Y. Wang, Y. P. Zhang, H. Li, L. Y. Yang, S. Y. Liao, W. Gu and X. Liu, *Journal of Materials Chemistry A*, 2016, **4**, 15494-15500.
16. G.-P. Li, G. Liu, Y.-Z. Li, L. Hou, Y.-Y. Wang and Z. Zhu, *Inorganic chemistry*, 2016, **55**, 3952-3959.